Human Molecular Genetics, 2015, Vol. 24, No. 3 **670–684**
doi:10.1093/hmg/ddu487
Advance Access published on September 30, 2014

Viral-mediated vision rescue of a novel AIPL1 cone-rod dystrophy model

Cristy A. Ku[1,2,*], Vince A. Chiodo[4], Sanford L. Boye[4], Abigail Hayes[2,3], Andrew F.X. Goldberg[5], William W. Hauswirth[4] and Visvanathan Ramamurthy[1,2,3,*]

[1]Center for Neuroscience, [2]Department of Ophthalmology and [3]Department of Biochemistry, Robert C. Byrd Health Sciences Center, West Virginia University, Morgantown, WV 26505, USA, [4]Department of Ophthalmology, University of Florida, Gainesville, FL 32610, USA and [5]Eye Research Institute, Oakland University, Rochester, MI 48309, USA

Received June 2, 2014; Revised August 15, 2014; Accepted September 22, 2014

Defects in *aryl hydrocarbon receptor interacting protein-like1* (*AIPL1*) are associated with blinding diseases with a wide range of severity in humans. We examined the mechanism behind autosomal dominant cone-rod dystrophy (adCORD) caused by 12 base pair (bp) deletion at proline 351 of hAIPL1 (P351Δ12) mutation in the primate-specific region of human AIPL1. Mutant P351Δ12 human isoform, aryl hydrocarbon receptor interacting protein-like 1 (*hAIPL1*) mice demonstrated a CORD phenotype with early defects in cone-mediated vision and subsequent photoreceptor degeneration. A dominant CORD phenotype was observed in double transgenic animals expressing both mutant P351Δ12 and normal hAIPL1, but not with co-expression of P351Δ12 hAIPL1 and the mouse isoform, aryl hydrocarbon receptor interacting protein-like 1 (mAipl1). Despite a dominant effect of the mutation, we successfully rescued cone-mediated vision in P351Δ12 *hAIPL1* mice following high over-expression of WT *hAIPL*1 by adeno-associated virus-mediated gene delivery, which was stable up to 6 months after treatment. Our transgenic P351Δ12 *hAIPL1* mouse offers a novel model of *AIPL1*-CORD, with distinct defects from both the *Aipl1*-null mouse mimicking LCA and the *Aipl1*-hypomorphic mice mimicking a slow progressing RP.

INTRODUCTION

Inherited retinal degeneration (IRD) is a group of blinding disorders affecting approximately 1 in 3000 people (1). Multiple forms of IRDs exist with diverse onset, symptoms, severity and progression of disease. Leber congenital amaurosis (LCA) shows the earliest onset and greatest severity of inherited retinal dystrophies, presenting in early infancy with severe visual impairment and absent or markedly reduced rod and cone-mediated electroretinograms (ERG) (2). Other IRDs such as retinitis pigmentosa (RP) and cone-rod dystrophy (CORD) show a greater variability in onset and rate of disease progression. RP patients present with night blindness as the first visual impairment alongside normal visual acuity. In contrast, CORD patients initially present with decreased visual acuity, central vision loss and dyschromatopsia, with progressive loss in peripheral, rod-mediated vision. Successful viral gene replacement therapy clinical trials improving visual function in LCA patients with defects in *retinal pigmented epithelium-specific 65kDa protein* (*RPE65*) have spurred efforts toward extending treatment for blinding diseases with slower progression and/or minimal photoreceptor loss such as CORD and RP (3–5).

One such candidate gene for future adeno-associated virus (AAV)-mediated gene replacement is *aryl hydrocarbon receptor interacting protein-like 1* (*AIPL1*) (6–9). Although defects in *AIPL1* are mainly associated with autosomal recessive LCA, *AIPL1* is also linked to less severe IRDs of CORD, juvenile RP, non-early onset RP and later onset retinal degeneration (6,10–12). These cases point to a subset of *AIPL1* patients who may be better candidates for gene replacement therapy due to a slower disease progression. Several non-LCA *AIPL1* cases are linked to defects in the C-terminal primate-specific proline-rich region of *AIPL1* (Fig. 1A, *gray box*), specifically mutations 12 base pair (bp) deletion at proline 351 of hAIPL1

*To whom correspondence should be addressed at: One Stadium Drive, West Virginia University Eye Institute, Morgantown, WV 26505, USA. Tel: +1-304598-4893; Fax: +1-304598-6928; Email: cku@mix.wvu.edu (C.A.K); Tel: +304-598-4860; Fax: +304-598-6928; Email: ramamurthyv@wvuhealthcare.com (V.R.)

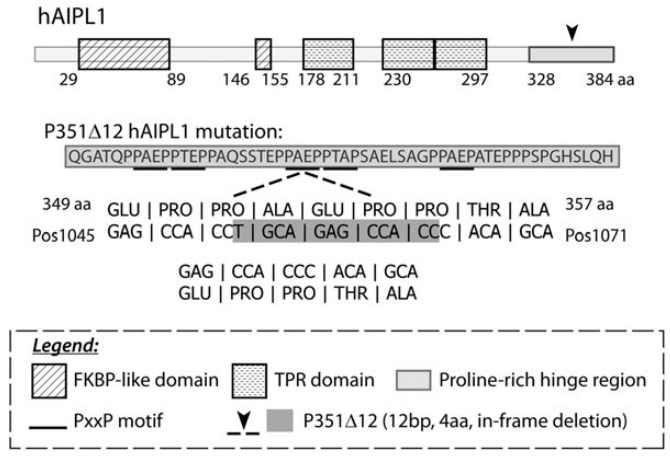

Figure 1. The P351Δ12 *hAIPL1* mutation interrupts a putative PxxP motif in the C-terminal proline-rich hinge region of hAIPL1. The 12 bp deletion (*arrowhead, dashed line* and *dark gray highlight*) results in a 4 amino-acid residue in-frame deletion, eliminating one of five potential PxxP motifs (*black underline*) present in the C-terminal proline-rich, primate-specific region (*light gray box*) of hAIPL1.

(P351Δ12; cDNA del1053–1064) and 2 bp deletion at alanine 336 of hAIPL1 (A336Δ2; cDNA del1008–1009) (10,13). P351Δ12 human isoform, aryl hydrocarbon receptor interacting protein-like 1 (*hAIPL1*) has been associated with autosomal dominant CORD and autosomal dominant juvenile RP (10). This finding indicates a dominant negative mechanism of dysfunction differing from the loss of function observed with truncation mutation stop truncation mutation at tryptophan 278 of hAIPL1 (W278X), the most common mutation found in patients (14). Autosomal dominance is also clinically important to examine as it indicates that AAV-mediated gene replacement may not be helpful for the P351Δ12 *hAIPL1* mutation, despite a slower disease progression. Lastly, it may shed light on the function of the C-terminal primate-specific proline-rich hinge region of AIPL1. The need for the hinge region in AIPL1 remains unknown, in spite of the prevalence of mutations in this region associated with blinding diseases (9,10,13).

The aim of this study was to evaluate the visual dysfunction and degeneration associated with the P351Δ12 *hAIPL1* patient mutation, to determine whether retinal degeneration occurs in a dominant fashion, and to attempt to rescue the visual dysfunction with AAV-mediated gene replacement. To do so, we generated transgenic mice expressing this hinge region mutation alongside control mice expressing wild-type (WT) *hAIPL1*, both expressed under the mouse *cone-rod homeobox* (*Crx*) promoter.

RESULTS

Generation of mouse models expressing WT *hAIPL1* and mutant P351Δ12 *hAIPL1*

Transgenic P351Δ12 *hAIPL1* mice were generated to examine the effects of the 12 bp, 4 amino acid residue in-frame deletion in the C-terminal proline-rich region of hAIPL1 (Fig. 1), on the function and survival of photoreceptor cells. A control transgenic line expressing WT *hAIPL1* (designated WT *hAIPL1*) was generated alongside the transgenic mutant line. Both WT and mutant transgene expression were driven by the 2.3 kilobase (kb) *mCrx* (cone-rod homeobox) promoter (Fig. 2A), active beginning at embryonic day 12.5 (E12.5) in retinal progenitor cells (15). The *mCrx* promoter was used due to its early expression activity in rod and cone photoreceptors (15), an important property because AIPL1 is necessary for rod and cone cell survival and function (16). Transgenic WT *hAIPL1* mice were backcrossed into mouse *Aipl1*-null mice to generate WT *hAIPL1* ($mAipl1^{+/-}$) (designated as WT *hAIPL1* (+/−)) and WT *hAIPL1* ($mAipl1^{-/-}$) (designated as WT *hAIPL1* (−/−)) littermates. Experimental P351Δ12 *hAIPL1* transgenic mice underwent a similar breeding scheme to generate P351Δ12 *hAIPL1* ($mAipl1^{+/-}$) (designated as P351Δ12 *hAIPL1* (+/−)) and P351Δ12 *hAIPL1* ($mAipl1^{-/-}$) (designated as P351Δ12 *hAIPL1* (−/−)). Mice from both lines were normal, healthy and fertile, with no gross morphological abnormalities. All comparisons are subsequently made between control WT *hAIPL1* (−/−) and experimental P351Δ12 *hAIPL1* (−/−) and are henceforth referred to as WT *hAIPL1* and P351Δ12 *hAIPL1* unless otherwise explicitly stated. The comparison between WT and mutant human AIPL1 necessitated the generation and comparison of two transgenic lines rather than littermates, because the mouse isoform lacks the C-terminal proline-rich region of interest. Additionally, generation of our control WT line allowed us to rule out potential effects stemming solely from the *mCrx* gene promoter and N-terminal Flag tag.

Protein expression of P351Δ12 hAIPL1 was comparable to WT hAIPL1 (Fig. 2B). As expected due to a 4 amino acid residue deletion, the mobility of mutant P351Δ12 hAIPL1 was shifted, running slightly below WT hAIPL1 in immunoblots. Additionally, with an AIPL1 antibody that recognizes both human and mouse isoforms equally (gift from Dr Tiansen Li), we observed that expression of WT and mutant hAIPL1 is greater than twice that of endogenous mouse isoform, aryl hydrocarbon receptor interacting protein-like 1 (mAipl1) present when measured in transgene positive *mAipl1* heterozygous ($mAipl1^{+/-}$) mice (Fig. 2B, *lanes 1 and 6, WT hAIPL1* $mAipl1^{+/-}$ *and P351Δ12 hAIPL1* $mAipl1^{+/-}$*, respectively*). WT *hAIPL1* mice showed comparable ERG responses to $mAipl1^{+/-}$ mice from P15 to P125 (Supplementary Material, Fig. S1), and *mAipl1* heterozygous mice ($mAipl1^{+/-}$), importantly, show no visual dysfunction or retinal degeneration (17).

Transgenically expressed WT and mutant P351Δ12 hAIPL1 were present in photoreceptor inner segments, as observed through segregation from co-labeled rhodopsin, a rod outer segment (ROS) protein (Fig. 2C) (16). WT and P351Δ12 hAIPL1 were also present in cone inner segments, as observed by co-labeling with peanut agglutinin (PNA), which stains cone membrane sheaths (Fig. 2D). This is in agreement with earlier observations of rod and cone expression of transgenes under the control of the *mCrx* promoter (15).

Progressive degeneration of photoreceptors in P351Δ12 *hAIPL1* mice

Retinal degeneration in mutant P351Δ12 *hAIPL1* mice was assessed through longitudinal immunohistochemistry studies with propidium iodide (PI, *red*), a nuclear marker that stains apoptotic cells prominently. Cone arrestin (cArr, *green*) was

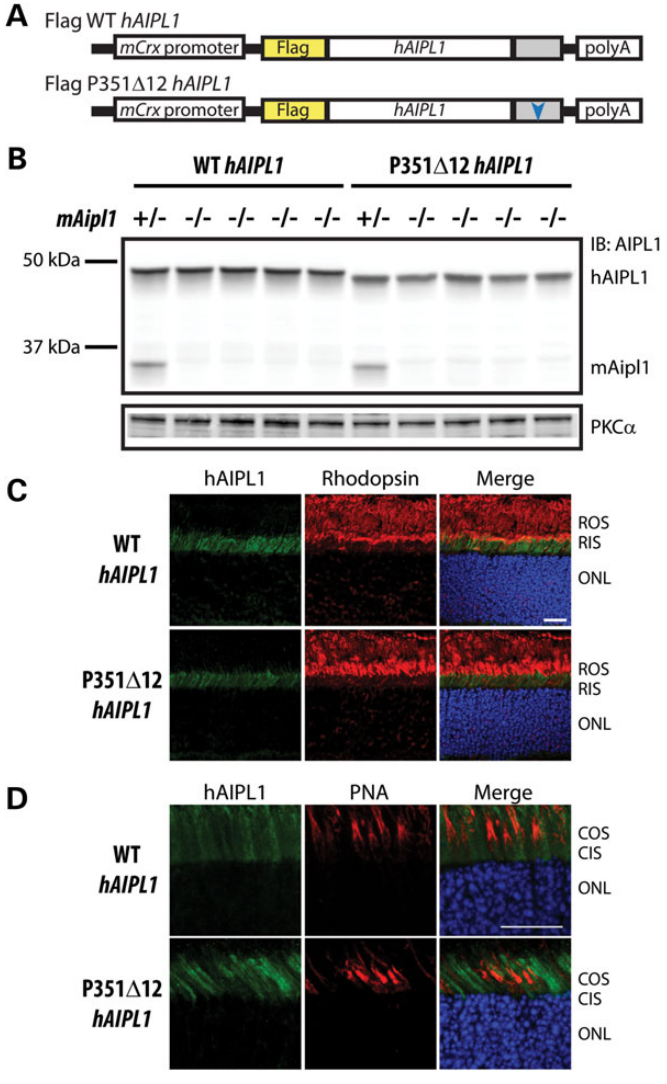

Figure 2. Comparable levels of AIPL1 expression and proper localization in transgenic P351Δ12 *hAIPL1* and control WT *hAIPL1* mice. (**A**) Transgenic mice were generated expressing either N-terminal Flag-tagged WT *hAIPL1* (control transgenic line) or Flag-tagged P351Δ12 *hAIPL1* (experimental transgenic line) under the 2.3 kb *mCrx* promoter. (**B**) Immunoblot of P16 retinal lysates from transgenic WT *hAIPL1* and P351Δ12 *hAIPL1* mice probed with anti-AIPL1 that recognizes both mouse and human AIPL1 equally (gift from Dr Tiansen Li), and anti-PKCα serves as a loading control. Equal amounts of protein were loaded for each sample (150 μg). mAipl1, mouse Aipl1; hAIPL1, human AIPL1; PKCα, protein kinase C α-type. Immunocytochemistry of hAIPL1 (*green*) co-labeled with (**C**) rhodopsin (*red*), a rod-specific marker and (**D**) PNA (*red*), which stains cone membrane sheaths. Cell nuclei are stained with DAPI (*blue*). ROS, rod outer segment; RIS, rod inner segment; ONL, outer nuclear layer; COS, cone outer segment; CIS, cone inner segment. Scale bar, 20 μm.

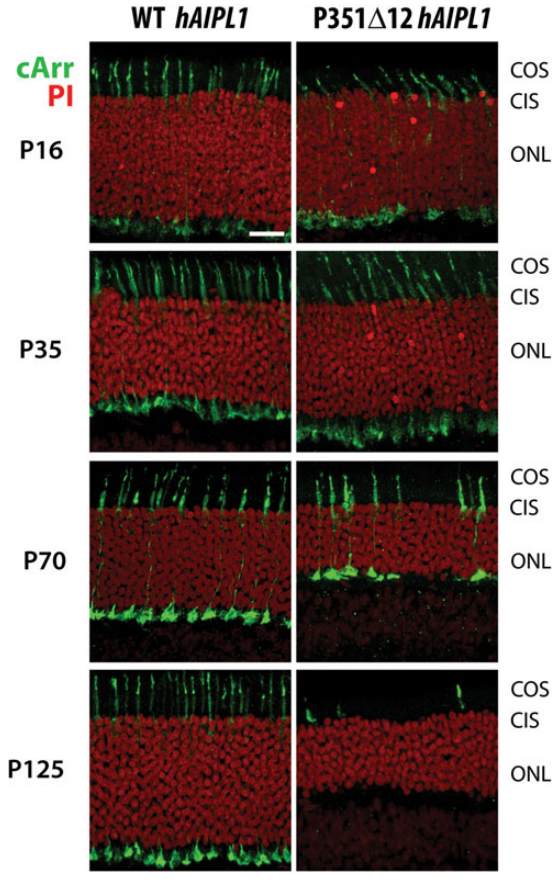

Figure 3. Slow and progressive degeneration of cone photoreceptors. Longitudinal survey of cell death, ONL thickness and cone cell survival from postnatal day 16 (P16) to P125. Cell death is observed at P16 with PI (*red*) particularly in the upper portion of the ONL where cone nuclei reside. Cones are visualized with an antibody against cArr (*green*). COS, cone outer segment; CIS, cone inner segment; ONL, outer nuclear layer. Scale bar, 20 μm.

co-labeled to assess progression of cone photoreceptor loss (Fig. 3). Despite occasional cell death observed at P16 and P35 in mutant mice, outer nuclear layer (ONL) thickness and number of cone photoreceptors remained similar to WT *hAIPL1* mice at P35 (Fig. 3). However, by P70, there was a noticeable decrease in ONL thickness and cone cell number, with an estimated loss of four to five cell layers and 40–50% loss of cones. A nearly complete cone cell loss was observed at P125, and although ONL thickness was relatively stable in the central retina between P70 and P125 as shown (Fig. 3), ONL thickness in the peripheral retina was decreased to four to five cell layers with estimated loss of 43% of outer nuclei (Supplementary Material, Fig. S2).

The outer segment (OS) length of photoreceptors expressing P351Δ12 *hAIPL1* was comparable to WT *hAIPL1* animals, as assessed through light microscopy (Supplementary Material, Fig. S3A). Ultrastructurally, rod (ROS) and cone outer segments (COS) in P351Δ12 *hAIPL1* mice appeared normal at P30 (Supplementary Material, Fig. S3B–D). These ultrastructural findings indicate normal rod and cone photoreceptor development in P351Δ12 *hAIPL1* animals prior to significant degeneration.

P351Δ12 *hAIPL1* mice show drastically reduced photopic responses and reduced scotopic responses at an early age

Electroretinography (ERG) was performed at P15, shortly after eyelid opening in mice, to evaluate whether the P351Δ12 *hAIPL1* mutation leads to visual deficits. P351Δ12 *hAIPL1* mice had markedly reduced photopic, cone-mediated ERG

responses, with approximately 30–40% of ERG responses from WT *hAIPL1* mice ($P < 0.0005$ at all light intensity comparisons; WT *hAIPL1* $n = 5$; P351Δ12 *hAIPL1* $n = 4$) (Fig. 4A and C, *left*). Scotopic, rod-mediated ERG responses were also reduced, although less drastically, to approximately 50–70% of WT *hAIPL1* ERG levels, with greater reduction at lower flash intensities (Fig. 4B and C, *right*) (*P* values as indicated, ranging from $P < 0.05$ to $P < 0.0005$). We therefore examined the intensity–response relationship from scotopic ERG measurements and found that rods from mutant P351Δ12 *hAIPL1* mice had a higher half-saturating light intensity compared with WT *hAIPL1* (Fig. 4D) (P351Δ12 *hAIPL1* $I_h = 0.05774 \pm 0.004798$ cd s/m^2; WT *hAIPL1* $I_h = 0.03346 \pm 0.003360$ cd s/m^2), indicating reduced sensitivity in mutant P351Δ12 *hAIPL1* mice.

P351Δ12 *hAIPL1* mice show decreased levels of phosphodiesterase 6

To investigate defects associated with decreased ERG responses, we examined levels of major phototransduction proteins in mutant P351Δ12 *hAIPL1* mice as compared with control WT *hAIPL1* mice. Semi-quantification of protein levels were conducted at P16, an age where OSs are well-formed and prior to significant retinal degeneration in P351Δ12 *hAIPL1* mice. The expression of rod outer segment membrane protein 1 (Rom1), an OS structural protein in rods and cones, and rhodopsin, a ROS protein, was unaltered. In addition, expression of protein kinase C, alpha subunit (PKCα), a protein expressed in bipolar cells, remained the same in retinal extracts from WT *hAIPL1* and P351Δ12 *hAIPL1* mice. These findings served as loading controls and also confirmed a lack of significant retinal degeneration and OS loss (Fig. 5A and B).

We observed a specific decrease in rod phosphodiesterase, alpha subunit (rod) (PDEα), phosphodiesterase, beta subunit (PDEβ) and phosphodiesterase, gamma subunit (PDEγ), in contrast to comparable levels of rod transducin (G-protein transducin alpha 1 subunit (rod), Gαt1) (Fig. 5A and B, *blue*) ($P < 0.0005$, paired *t*-test, *black asterisks*). The decrease in PDEγ was more pronounced in comparison to the equimolar decreases of PDEα and β (one-way analysis of variance (ANOVA) with multiple comparisons test: PDEα versus PDEβ, $P = 0.2759$; PDEα versus PDEγ, $P < 0.0005$; PDEβ versus PDEγ, $P < 0.005$) (Fig. 5A and B, ANOVA *P*-values, *purple asterisks*). In examining cone-specific proteins (Fig. 5A and B, *red*), we observed a decrease in cone phosphodiesterase, alpha prime subunit (PDEα′) and cone transducin (Gαt2 = G-protein transducin alpha 2 subunit (cone), Gαt2), whereas red/green opsin (R/G op) levels were equivalent between WT and mutant P351Δ12 *hAIPL1* mice. Rom1 and guanylyl cyclase-E (GC-E), present in rods and cones (Fig. 5A and B, *green*), were also unaltered in P351Δ12 *hAIPL1* mice.

Although rod and cone PDE subunits showed decreased expression in mutant P351Δ12 *hAIPL1* mice as compared with control WT *hAIPL1* mice, they were properly localized to ROS and COS, respectively (Fig. 6B and D). Additionally, rod transducin (Gαt1, Fig. 6A) and red/green opsin (R/G op, Fig. 6C), which showed normal proteins levels, also localized properly to the OSs.

Rapid and progressive loss of visual response in animals expressing P351Δ12 hAIPL1

To evaluate whether visual defects were progressive or stationary, we measured ERG responses in animals of increasing age. P351Δ12 *hAIPL1* mice showed a rapid decline in photopic cone-mediated ERG responses decreasing to approximately 10% of WT *hAIPL1* levels by P60 (Fig. 7A, *solid line*). Scotopic, rod-mediated ERG responses also decreased albeit at a much slower rate (Fig. 7A, *dashed line*). The largest decline in scotopic response in P351Δ12 *hAIPL1* mice was observed between P60 and P90, which then remained stable until P360 (data not shown).

To evaluate whether decreased ERG responses affected functional vision in mutant P351Δ12 *hAIPL1* mice, we performed behavioral tests based on the ability of the mouse to reflexively track computer-generated sinusoidal gratings (19). Visual acuity is evaluated by measuring the threshold (maximal) spatial frequency of the gratings that elicits an optokinetic response (OKR) from the mouse under photopic and scotopic conditions (20), with higher maximal spatial frequencies suggesting greater visual acuity. At P30, P351Δ12 *hAIPL1* mice showed significantly lower threshold spatial frequencies than WT *hAIPL1* mice under photopic conditions (Fig. 7B, photopic *left*) ($P < 0.05$; WT mean $= 0.5339 \pm 0.03541$ cyc/deg, $n = 5$; P351Δ12 mean $= 0.3724 \pm 0.02983$ cyc/deg, $n = 5$). Photopic response further worsened at P60 in mutant mice (Fig. 7C, photopic *left*) ($P < 0.0005$; WT mean $= 0.4303 \pm 0.02076$ cyc/deg, $n = 5$; P351Δ12 mean $= 0.1210 \pm 0.01990$ cyc/deg, $n = 5$). The decrease in photopic response between P30 and P60 was significant in mutant P351Δ12 but not WT *hAIPL1* mice (paired *t*-test, $P < 0.005$ for P351Δ12 P30 mean $= 0.3724 \pm 0.02983$ cyc/deg versus P351Δ12 P60 mean $= 0.1210 \pm 0.01990$ cyc/deg, $n = 5$; $P > 0.05$ for WT P30 mean $= 0.5339 \pm 0.03541$ cyc/deg versus WT P60 mean $= 0.4303 \pm 0.02076$ cyc/deg, $n = 5$). Under scotopic conditions, mutant P351Δ12 mice showed a trend toward lower acuity than WT mice, with significantly lower spatial frequencies under three of five scotopic background light intensities at P30 (Fig. 7B, scotopic *right*) (*P* values ranging from $P < 0.05$ to $P < 0.005$; WT $n = 5$; P351Δ12 $n = 5$). By P60, visual behavior was significantly lowered in animals expressing mutant *hAIPL1* under all scotopic light intensities (Fig. 7C, scotopic right) ($P < 0.0005$; WT $n = 5$; P351Δ12 $n = 5$).

Animals expressing P351Δ12 hAIPL1 exhibit dominant visual deficits

To address whether the P351Δ12 *hAIPL1* mutation acts in a dominant fashion, we generated double transgenic mice by crossing WT *hAIPL1* with P351Δ12 *hAIPL1* transgenic mice, which were both flag-tagged at the N-terminus of AIPL1 (Fig. 2A). Double transgenic animals co-expressing WT and P351Δ12 hAIPL1 (Fig. 8A and B, *blue* and *red* waveforms) showed a persistent defect in cone-mediated ERG responses similar to that in mutant P351Δ12 *hAIPL1* mice, as compared with a littermate expressing WT hAIPL1 at P120 (Fig. 8A and B, *black* waveforms). The dominant effects of P351Δ12 hAIPL1 was also present in rods in double transgenic mice. Rod-mediated ERG responses of double transgenic *hAIPL1* mice were generally comparable to mutant P351Δ12 *hAIPL1*, with both significantly lower than

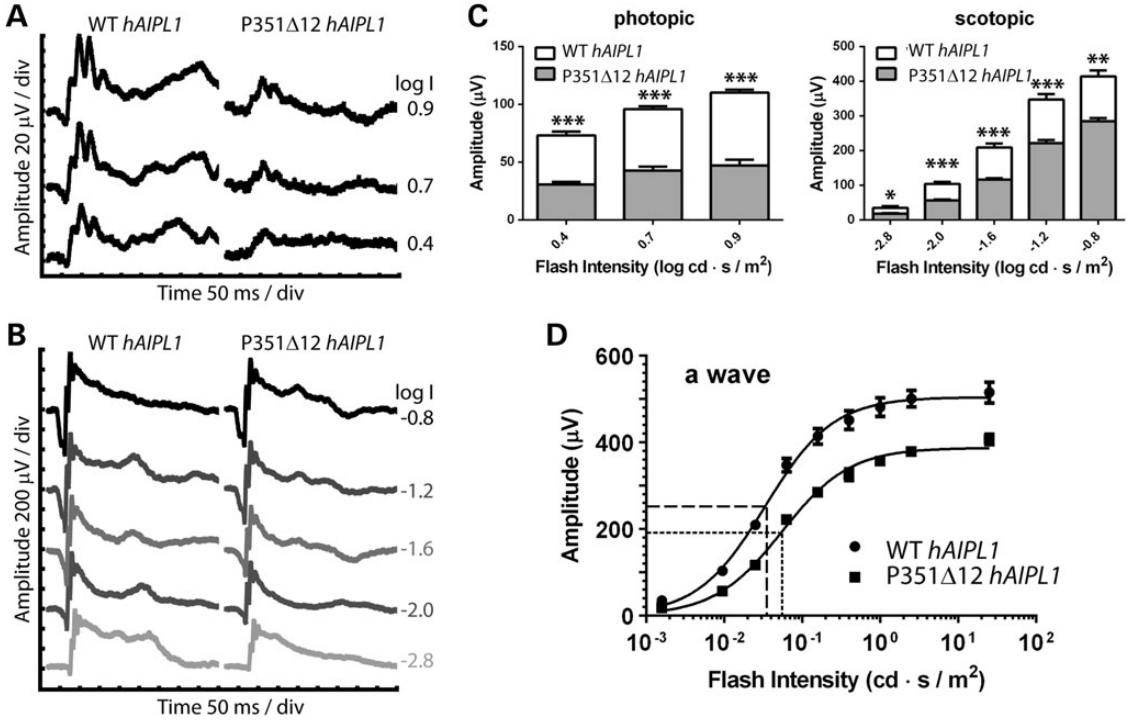

Figure 4. Mice expressing P351Δ12 *hAIPL1* mutation show an early dramatic decrease in photopic vision and defects in scotopic vision. Families of representative ERG responses from postnatal day 15 (P15) WT *hAIPL1* and mutant P351Δ12 *hAIPL1* mice, as recorded under (**A**) photopic, cone-mediated and (**B**) scotopic, rod-mediated conditions with flashes of indicated light intensities (log cd s/m^2). (**C**) Comparison of mean cone (*b*-wave amplitudes) and rod (*a*-wave amplitudes) photoreceptor responses between WT (*white bar*; $n = 5$) and P351Δ12 *hAIPL1* (*gray bar*; $n = 4$). Average amplitudes ($\pm$ SEM) from WT *hAIPL1* mice were significantly different from P351Δ12 *hAIPL1* mice at all photopic and scotopic flash intensities, with *P* values indicated as: $^{*}P < 0.05$, $^{**}P < 0.005$, $^{***}P < 0.0005$. (**D**) Intensity–response relationship for scotopic *a*-wave amplitude, where data were fitted with hyperbolic function (18), $A = A_{\max}((I^n)/(I^n + I_h^n))$, where $A_{\max}$ is the maximal *a*-wave amplitude, n is the Hill coefficient and I_h is the half-saturating light intensity. This curve fit yielded scotopic *a*-wave half-saturating light intensities of 0.03346 $\pm$ 0.003360 cd s/m^2 (WT *hAIPL1*, $n = 5$) and 0.05774 $\pm$ 0.004798 cd s/m^2 (P351Δ12 *hAIPL1*, $n = 4$). Data points are mean $\pm$ SEM.

WT *hAIPL1* mice. (Fig. 8C, scotopic) (*P* values as indicated $^{**}P < 0.005$, $^{****}P < 0.0001$; $n = 4$ for each group). These effects were seen despite expression of P351Δ12 hAIPL1 being 5- to 10-fold less than WT hAIPL1, as compared with the equivalent levels of WT and mutant P351Δ12 hAIPL1 in the respective single transgenic mice (Fig. 8A, *Double Tg: 1 blue* and *2 red*, control *Flag WT* and *Flag Mut*).

In contrast to co-expression of WT and mutant human AIPL1, no ERG defects are observed when mouse Aipl1 is co-expressed with mutant hAIPL1, as P351Δ12 *hAIPL1*+ *mAipl1*+/− mice (Fig. 9A, *green*) show equivalent photopic and scotopic ERG responses to control transgene negative *mAipl1*+/− mice at P120 (P351Δ12 *hAIPL1*− *mAipl1*+/− mice, Fig. 9A, *orange*). Transgenic P351Δ12 *hAIPL1*+ *mAipl1*−/−, the model of degeneration used for all experiments, is shown here for comparison (Fig. 9A, *purple*). In all cases, there was no significant difference between P351Δ12 *hAIPL1*+ (*mAipl1*+/−) and the control P351Δ12 *hAIPL1*− (*mAipl1*+/−) (*white bar*), and significant differences between both groups to the degeneration model, P351Δ12 *hAIPL1*+ (*mAipl1*−/−) (*gray bar*) (*P* values ranging from $P < 0.05$ to $P < 0.0001$; $n = 3$ for each group).

AAV-mediated gene delivery of WT *hAIPL1* into mutant P351Δ12 *hAIPL1* mice rescues cone defects

We introduced WT hAIPL1 through AAV-mediated gene delivery into P351Δ12 *hAIPL1* mice, using a previously published self-complementary Y733F tyrosine capsid mutant AAV2/8 viral vector expressing *hAIPL1* under a human rhodopsin kinase (*RK*) promoter (self-complementary Y733F tyrosine capsid mutant adeno-associated virus serotype 2/8, expressing hAIPL1 under the RK promoter, scAAV2/8-Y733F-p*RK-hAIPL1*) (21). The RK promoter is active in both rods and cones in mice (22–24). Following viral-mediated gene delivery at P10 into P351Δ12 *hAIPL1* mice, we surprisingly observed rescue of photopic cone-mediated ERG responses in the treated eye when directly compared with the contralateral untreated eye at P30 ($P < 0.005$, paired *t*-test; untreated mean = 10.00 $\pm$ 3.751 μV, $n = 6$; treated mean = 46.33 $\pm$ 8.131 μV, $n = 6$) (Fig. 10A). Rescue effects on cone-mediated ERG responses following one AAV-treatment administered at P10 were maintained at P130, with no statistically significant difference between cone ERG responses from P30 to P130 (paired *t*-test; P30 mean = 43.4 $\pm$ 9.29 μV; P130 mean = 32.6 $\pm$ 6.08 μV; $P = 0.2588$, $n = 5$). Visual acuity in photopic conditions was improved in treated eyes compared with untreated eyes, as OKRs were present at higher spatial frequencies at P30 ($P < 0.05$, paired *t*-test; untreated mean = 0.09625 $\pm$ 0.06172 cyc/deg, $n = 4$; treated mean = 0.4278 $\pm$ 0.09206 cyc/deg, $n = 4$) (Fig. 10C). In contrast to photopic responses, scotopic rod-mediated ERG responses did not improve with AAV-mediated gene delivery of WT hAIPL1 ($P > 0.05$; untreated mean = 95.50 $\pm$ 14.34 μV; treated mean = 57.67 $\pm$ 13.10 μV, $n = 5$) (Fig. 10B).

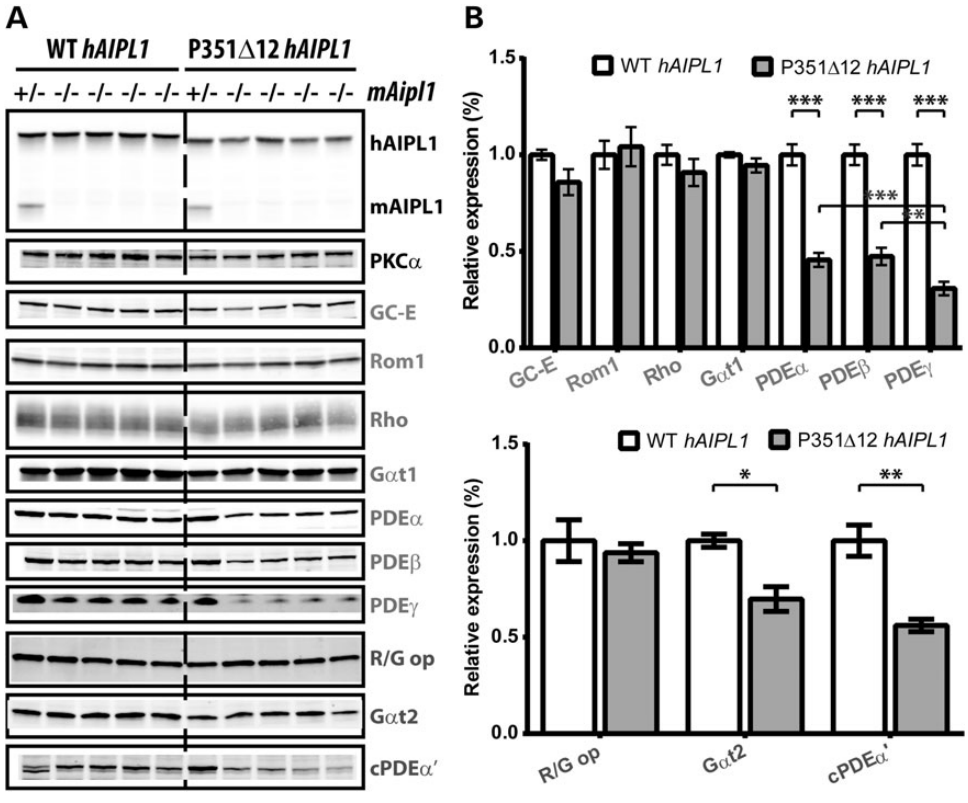

Figure 5. P351Δ12 *hAIPL1* mutant mice show decreased rod and cone phosphodiesterase 6. (**A**) Immunoblots from P16 retinal lysates from transgenic WT *hAIPL1* and P351Δ12 *hAIPL1* mice. One transgenic positive *mAipl1* heterozygous mouse was included as a littermate control (lanes 1 and 6). Equal amounts of protein (150 μg) were loaded for each sample, and western blots were probed with the indicated antibodies. Antibodies were used to examine proteins that are present in both rods and cones (GC-E, Rom1), rod-specific (Rho, Gαt1, PDEα, PDEβ, PDEγ) or cone-specific (R/G op, Gαt2, cPDEα′). PKCα, present in rod bipolar cells of the inner nuclear layer, is used as a loading control. (**B**) Quantification of relative expression of proteins expressed as a fraction of the average obtained from WT *hAIPL1* (*mAipl1*$^{-/-}$) mice. hAIPL1, human AIPL1; mAipl1, mouse Aipl1; PKCα, protein kinase C α-type; GC-E, guanylyl cyclase-E; Rom1, retinal outer membrane protein 1; Rho, rhodopsin; Gαt1, guanine nucleotide binding protein (G protein) α transducing 1 subunit, commonly known as rod transducin α-subunit; PDEα, cyclic guanosine monophosphate (cGMP) phosphodiesterase 6 α-subunit; PDEβ, cGMP phosphodiesterase 6 β-subunit; PDEγ, cGMP phosphodiesterase 6 γ-subunit; R/G opsin, cone red/green opsin; Gαt2, cone transducin α-subunit; cPDEα′, cone cGMP phosphodiesterase α′-subunit. *P* values are indicated as follows: $^{*}P < 0.05$, $^{**}P < 0.005$, $^{***}P < 0.0005$.

Immunocytochemistry conducted at P130 showed clear and long-term rescue of cone photoreceptors in treated eyes as directly compared with contralateral untreated eyes, with COS labeled with PNA (Fig. 11A, PNA, *red*) and cArr (Fig. 11B, cArr, *red*). Additionally, cPDEα′ expression was restored, which was specifically decreased in mutant P351Δ12 *hAIPL1* mice (Fig. 11A, cPDEα′, *green*). Cone rescue was also confirmed in immunoblots with direct comparisons between the uninjected eye (UE) and injected eye (IE) from four individual mice, where cone-specific proteins, cone transducin and cPDEα′, are observed at higher levels in the IE compared with a lack or low expression of proteins in the contralateral UE (Fig. 11E and F). Rod PDEα and PDEβ expression showed a near statistically significant increase in treated eyes as directly compared with its untreated eye (Fig. 11E and F) (paired *t*-test, $P = 0.07$). Interestingly, however, rod PDEγ levels were nearly identical, with no uninjected and injected pairs showing an increase in protein levels (Fig. 11E and F). Immunocytochemistry examining rod PDEβ and PDEγ confirmed trends observed in immunoblots (Fig. 11C and D).

To resolve the difference observed between introduction of WT *hAIPL1* through AAV-mediated gene delivery as compared with genetic manipulation, protein expression of WT hAIPL1 was compared between the two methods. We observed a drastically greater expression of WT hAIPL1 in AAV-treated eyes than double transgenic mice (Fig. 12). Although the WT hAIPL1 band could not be fully resolved from the Flag P351Δ12 hAIPL1 band in AAV-treated eyes, we estimate (non-tagged) WT hAIPL1 to be in 40- to 50-fold excess of mutant P351Δ12 hAIPL1 (Fig. 12, *lanes 7–9*), whereas Flag WT hAIPL1 in double transgenic mice are in about 5-fold excess of Flag P351Δ12 hAIPL1 (Fig. 12, *lanes 1–3*).

DISCUSSION

The P351Δ12 *hAIPL1* mutation has been reported in two probands, both of whom inherited the mutation in an autosomal dominant manner (10). The two patients, however, had discordant diagnoses; one with CORD and the other with juvenile RP. To examine this mutation in the C-terminal proline-rich domain of *hAIPL1*, we generated a transgenic P351Δ12 *hAIPL1* mouse model, which exhibited a CORD phenotype with early loss of cone-mediated vision and subsequent cone

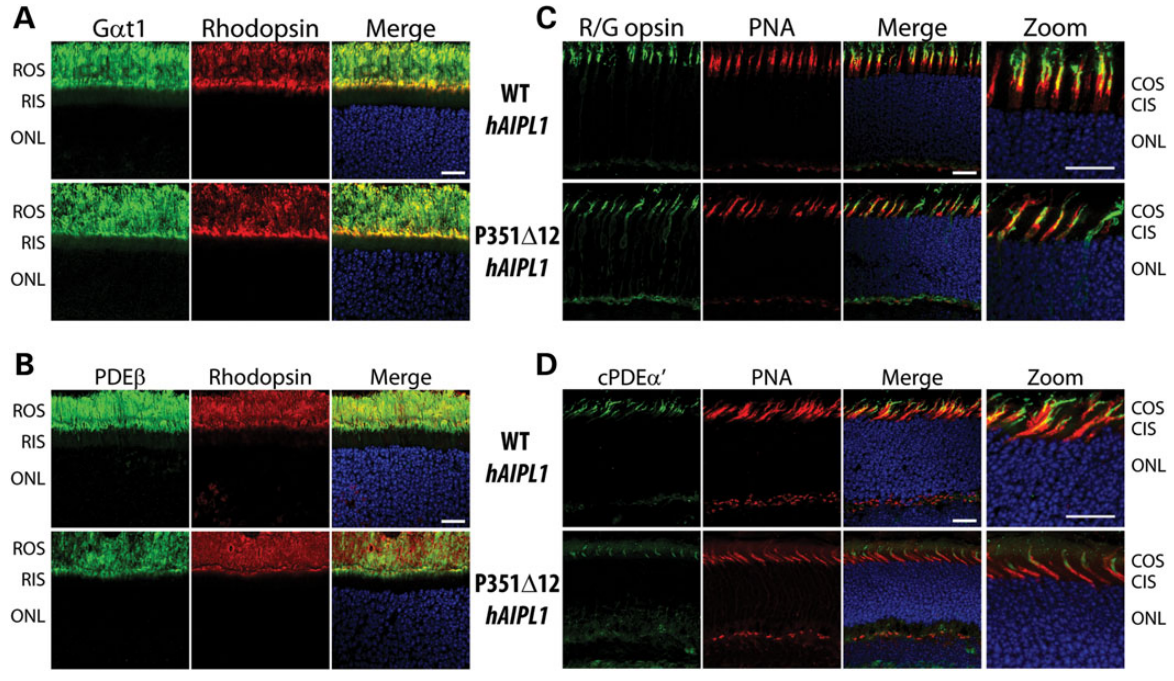

Figure 6. Rod and cone phosphodiesterase 6 in P351Δ12 *hAIPL1* mutant mice is decreased but localized properly. Immunocytochemistry of cryosections from P16 WT *hAIPL1* and P351Δ12 *hAIPL1* mice of rod-specific proteins, (**A**) Gαt1 (*green*), and (**B**) PDEβ (*green*), co-labeled with rhodopsin (*red*), present in ROSs. Immunocytochemistry of cone-specific proteins, (**C**) red/green opsin (R/G opsin, *green*), and (**D**) cPDEα′ (*green*), co-labeled with PNA (*red*), which stains cone membrane sheaths. Cell nuclei are stained with DAPI (*blue*). Gαt1, guanine nucleotide binding protein (G protein) α transducing 1 subunit, commonly known as rod transducin α-subunit; PDEβ, cGMP phosphodiesterase 6 β-subunit; R/G opsin, red/green opsin; cPDEα′, cone cGMP phosphodiesterase α′-subunit; ROS, rod outer segment; RIS, rod inner segment; ONL, outer nuclear layer; COS, cone outer segment; CIS, cone inner segment. Scale bar, 20 μm.

photoreceptor degeneration. Cone-mediated ERG response was reduced by 60% at P15 that progressed to a dramatic 90% loss by P70 in mutant mice. However, 50–60% of cone photoreceptors persisted at P70 and complete loss of cone cells in mutant mice did not occur until P120. In comparison to photopic vision, rod-mediated ERGs declined slowly in mutant animals and plateaued at 40% of ERG response in control animals expressing WT *hAIPL1* by P120 with persistence of four to seven cell layers, which were all presumably rod photoreceptors due to complete cone degeneration by P120. The disparity between low visual responses and persistent photoreceptor survival, particularly with cone photoreceptors, indicated substantial opportunity for vision rescue. We also did not observe any ultrastructural defects in rods or cones that may account for low visual responses.

Indeed, AAV-mediated over-expression of WT *hAIPL1* in mutant P351Δ12 *hAIPL1* mice rescued cone-mediated vision with drastic improvement of photopic ERG responses. Cone PDEα′ and cone transducin (Gαt2) expression, deficient in mutant mice prior to degeneration, were restored after treatment. An increase in ONL by two to three cell layers was also observed with prolonged survival of cone photoreceptors at P120. Treated eyes in P351Δ12 *hAIPL1* mice however showed no appreciable improvement in scotopic rod-mediated vision despite robust expression of WT hAIPL1 protein. The gradual decrease in scotopic ERG responses and rod photoreceptor loss in P351Δ12 *hAIPL1* may have masked rescue effects. Alternatively, there was a trending increase in rod PDEα and β catalytic subunits but not rod PDEγ, although all three subunits were decreased at early postnatal ages before degeneration. Unimproved levels of rod PDEγ potentially explain persistently low rod-mediated ERG responses following treatment.

Cone rescue was unexpected with indications of a dominant negative effect of P351Δ12 *hAIPL1* on WT *hAIPL1* in cones of double transgenic mice. The mice completely lacked cone ERG responses despite roughly a 5-fold excess of WT over mutant hAIPL1. This is in concordance with the phenotype of heterozygous P351Δ12 *hAIPL1*-CORD patients. However, the higher 50-fold excess of WT over mutant P351Δ12 hAIPL1 achieved with AAV-treatment was able to outcompete the dominant negative effect of mutant hAIPL1 in cones. In contrast to cones, over-expression of WT hAIPL1 did not increase rod photoreceptor responses or levels of rod PDEγ, indicating that mutant P351Δ12 hAIPL1 may affect rod PDEγ levels in a negative manner independent of WT hAIPL1. Rod-mediated ERG defects were also present in double transgenic mice as compared with WT *hAIPL1* littermates. It appears that independent of the amount of WT hAIPL1 over mutant hAIPL1, 5-fold in double transgenic mice and 50-fold in AAV-treated mice, the presence of mutant hAIPL1 leads to rod deficits.

A recent study found that truncated human AIPL1 protein lacking the proline-rich domain had increased *in vitro* binding affinity to Hsp90, a potential co-chaperone heterocomplex protein for phosphodiesterase. Interestingly, an orally bioavailable inhibitor of Hsp90 has been shown to affect the stability of phosphodiesterase in retina suggesting the importance of Hsp90 levels in biosynthesis of rod phosphodiesterase (25). Altogether with results from this study, it suggests that aberrant interaction of Hsp90 by mutant AIPL1 leads to defective folding and assembly of rod phosphodiesterase (26). It remains unclear

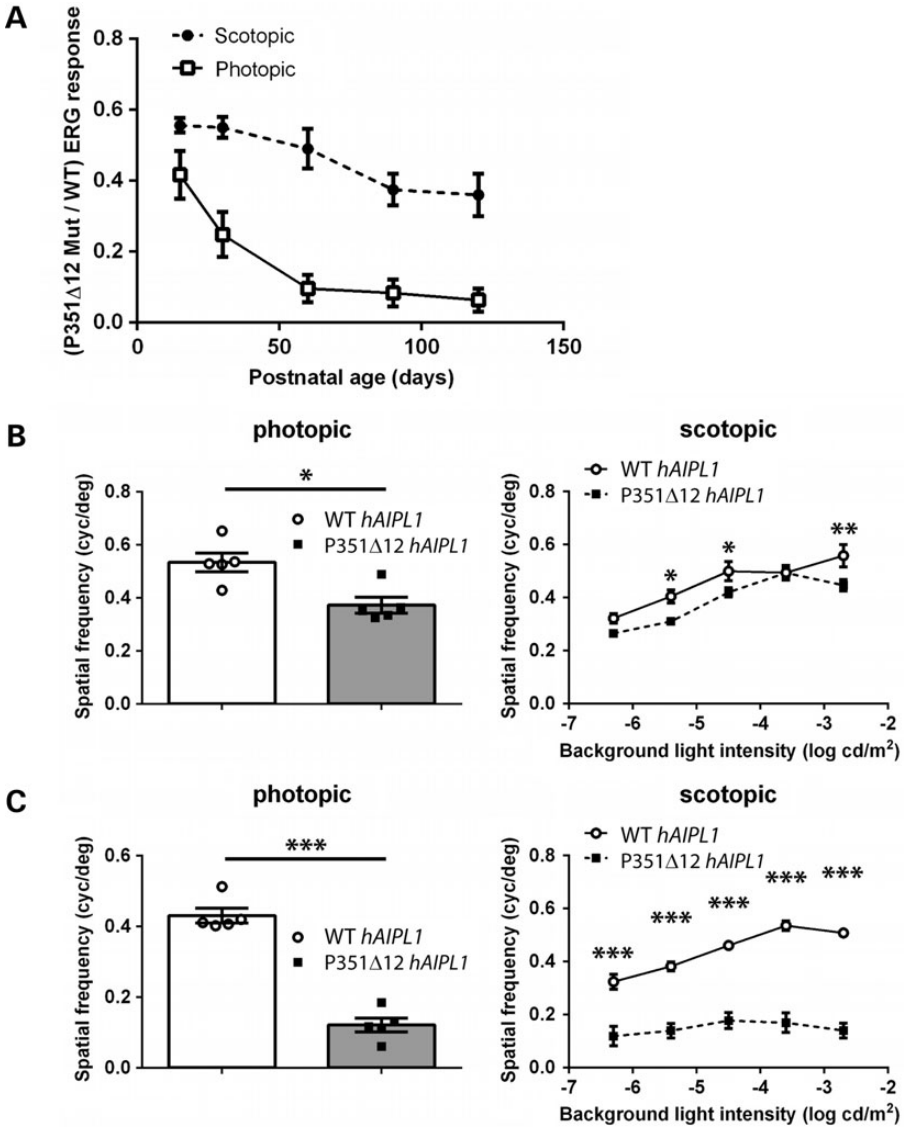

Figure 7. P351Δ12 *hAIPL1* mice show a rapid decline in photopic vision and slower decline of scotopic vision. (**A**) ERG responses over time (from P15 to P120), as expressed as the ratio of (P351Δ12 *hAIPL1*/WT *hAIPL1*) *a*-wave amplitudes, obtained from measurements taken with 2.5×10^{-2} cd s/m^2 flashes under scotopic, rod-mediated conditions (*dashed line* and *black circles*) and the ratio of (P351Δ12 *hAIPL1*/WT *hAIPL1*) *b*-wave amplitudes with 2.5 cd s/m^2 flashes under photopic, cone-mediated conditions (*solid line* and *white squares*) (P15, $n = 4$; P30, $n = 6$; P60, $n = 5$; P90, $n = 5$; P120, $n = 5$). (**B** and **C**) Functional vision as tested on Opto-Motry (Cerebral Mechanics, Inc.), measures the maximal spatial frequency (cyc/deg) eliciting an OKR under photopic and scotopic conditions, at (**B**) P30, and (**C**) P60. Maximal spatial frequencies of WT *hAIPL1* ($n = 5$) and P351Δ12 *hAIPL1* ($n = 5$) mice. Maximal spatial frequencies measured under photopic conditions of WT *hAIPL1 (white bar* and *white circles*) and mutant *hAIPL1* mice (*grey bar* and *black squares*), with data points representing values from individual mice (*white circles* and *black squares*). Multiple measurements were obtained across the indicated background light intensities under scotopic conditions, in WT *hAIPL1* (*solid line* and *white circles*) and mutant *hAIPL1* (*dashed line* and *black squares*). Bars represent mean ± SEM values. *P* values are indicated as follows: $^{*}P < 0.05$, $^{**}P < 0.005$, $^{***}P < 0.0005$.

what the specific effect of altered Hsp90 interaction is on rod PDEγ levels, which was persistently decreased despite increased rod PDEα and β in our studies. It is also not clear if an aberrant interaction of AIPL1 with Hsp90 will have a more severe effect on cone phosphodiesterase 6 (PDE6) in comparison to rod PDE6 to explain the rapid loss of cone response in our animal models. Current studies are underway to test the need for Hsp90 for the assembly or stability of cone PDE6 in cone-rich animal models. Ideally, these questions are better explored in a cell-culture system, but unfortunately there is no viable strategy for expression of functional, assembled PDE6. Therefore, *in vitro* binding studies using various purified AIPL1 mutants are needed to complement our studies and clarify the interplay between AIPL1 and Hsp90 chaperone complex in the biosynthesis of phosphodiesterase. These studies are also needed to evaluate whether the P351Δ12 hAIPL1 mutation has a similar effect on Hsp90 interaction as seen with complete deletion of the proline-rich region.

It remains unknown whether dominant negative effects are exerted through aberrant interaction between WT and mutant hAIPL1 or aberrant interaction with another protein. Our findings suggest that dominant negative effects are independent of

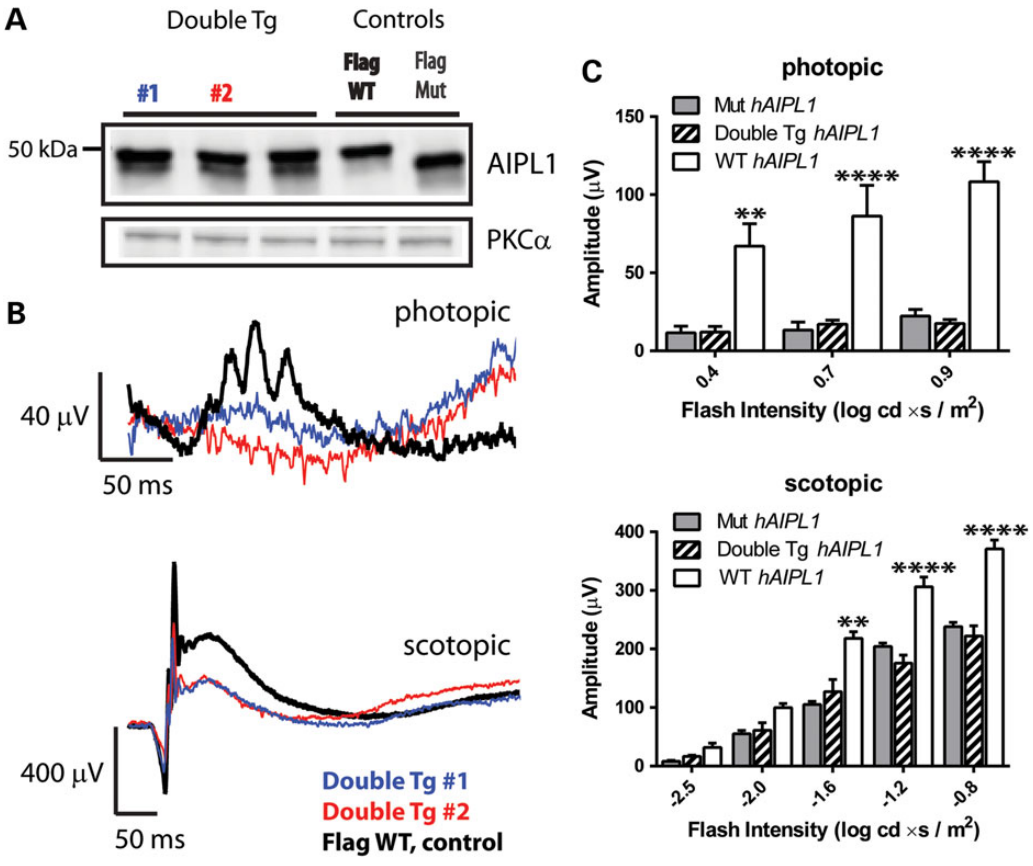

Figure 8. Dominant negative visual defects in mice co-expressing P351Δ12 hAIPL1 and WT hAIPL1 protein. (**A**) P351Δ12 *hAIPL1* mice were crossed with WT *hAIPL1* mice to generate double transgenic positive off-spring (*Double Tg*), and co-expression of protein was evaluated with anti-AIPL1 (top immunoblot) on a 9% polyacrylamide SDS-PAGE resolving gel of 16 cm height. Single transgenic mice controls (*Controls: Flag WT* and *Flag Mut* lanes) are run on the same gel to show the expected differences in size due to deletion of 4 amino acid residues. Loading control is shown with anti-PKCα (bottom immunoblot). (**B**) ERG responses at P120 from the corresponding individual mice shown in the immunoblot. Photopic and scotopic responses from a mouse expressing Flag WT hAIPL1 (*Flag WT* lane in immunoblot; *black* ERG waveforms), and two independent mice co-expressing Flag WT and Flag P351Δ12 hAIPL1 (*Double Tg #1, #2* in immunoblot; *blue* and *red* ERG waveforms). (**C**) Comparison of mean cone (*b*-wave amplitudes) and rod (*a*-wave amplitudes) (mean ± SEM) photoreceptor responses between mutant P351Δ12 *hAIPL1* (*gray bar*; $n = 4$), double transgenic *hAIPL1* (*striped bar*; $n = 4$), and WT *hAIPL1* mice (*white bar*; $n = 4$). Significant differences are present between WT *hAIPL1* to both double transgenic and mutant P351Δ12 *hAIPL1* mice, with *P* values indicated as follows: $^{**}P < 0.005$, $^{****}P < 0.0001$.

WT hAIPL1 in rods, and that the mechanism of dominant dysfunction may differ between rods and cones. Further detailed mechanistic studies are needed to shed light on these questions, including *in vitro* dimerization studies examining heterodimerization between mAipl1, WT hAIPL1 and mutant P351Δ12 hAIPL1. Our initial co-immunoprecipitation studies using proteins expressed in HEK293 tissue culture cells show homodimerization of hAIPL1 and no interaction between mAipl1 or between hAIPL1 and mAipl1 (Supplementary Material, Fig. S4), corresponding with our results showing no change in ERG response in animals co-expressing hAIPL1 and mAipl1 (Fig. 9). Further studies are needed to confirm these results *in vivo* in retinal tissue and to study the need for proline-rich region in dimerization and function of AIPL1. Additionally, future *in vivo* immunoprecipitation studies are needed to delineate aberrant interacting proteins to mutant hAIPL1 as compared with WT hAIPL1.

Although the exact alteration in the structure of the proline-rich domain is unknown, we demonstrate that the P351Δ12 hAIPL1 mutation affects the normal functioning of the region, potentially stemming from disruption of two of the five proline motifs (Fig. 1). However, future structural studies are required to definitively determine the effects of the P351Δ12 mutation on AIPL1 structure.

Ours is the first study to highlight and provide *in vivo* evidence of the importance of the C-terminal proline-rich region of human AIPL1. The findings from this work are in line with recent *in vitro* studies demonstrating the essential contribution of the proline-rich region to the chaperone function of AIPL1 in the folding of model proteins (26). Our *in vivo* model implicates distinct mechanisms of dysfunction exerted through mutant P351Δ12 hAIPL1 between rods and cones, which also differ from the loss of function commonly associated with AIPL1. AAV-mediated gene replacement dramatically rescued cone-mediated vision, which is particularly vital for central macular vision in patients. Rescue of rods may necessitate dual targeting with downregulation of the mutated gene followed by gene replacement.

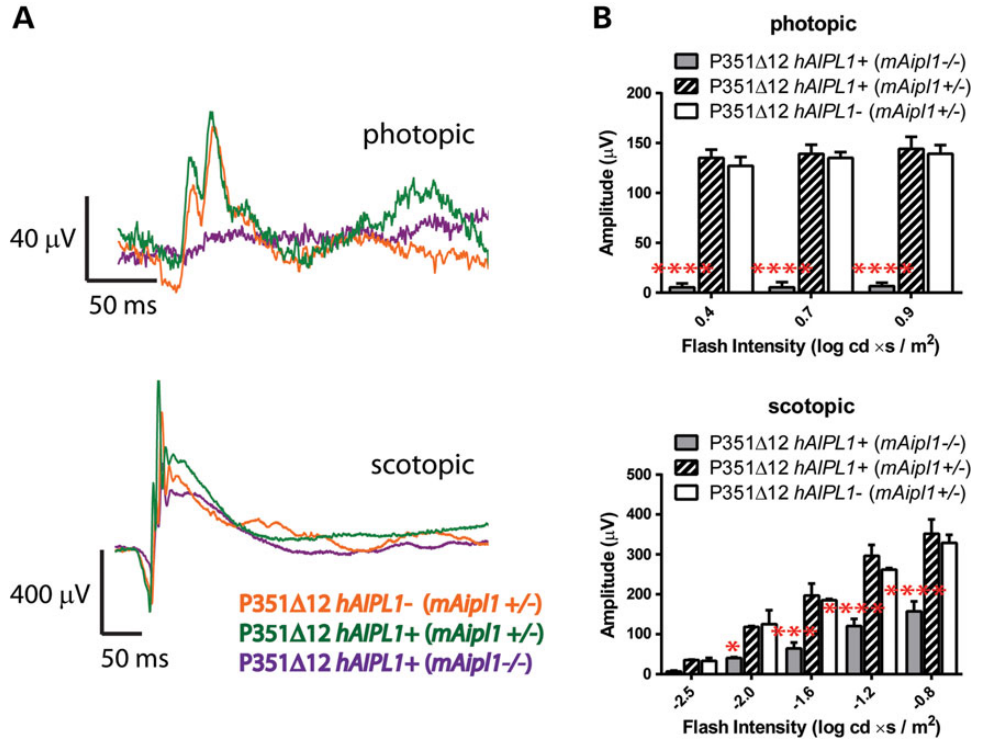

Figure 9. P351Δ12 hAIPL1 expression does not affect visual response in animals expressing mAipl1. (**A**) Representative photopic and scotopic ERG responses from P120 P351Δ12 *hAIPL1*− (*mAipl1*+/−) (*orange* waveforms), P351Δ12 *hAIPL1*+ (*mAipl1*+/−) (*green* waveforms) and P351Δ12 *hAIPL1*+ (*mAipl1*−/−) (*purple* waveforms) littermates. Photopic responses were obtained with 2.5 cd s/m^2 flashes under cone-mediated conditions, and scotopic responses were obtained with 2.5 × 10^{-2} cd s/m^2 flashes under rod-mediated conditions. (**B**) Comparison of mean cone (*b*-wave amplitudes) and rod (*a*-wave amplitudes) photoreceptor responses between P351Δ12 *hAIPL1*+ (*mAipl1*−/−) (*gray bar*), P351Δ12 *hAIPL1*+ (*mAipl1*+/−) (*striped bar*) and P351Δ12 *hAIPL1*− (*mAipl1*+/−) (*white bar*) (mean ± SEM). In all scotopic and photopic flash intensities, there was no significant difference between P351Δ12 *hAIPL1*− (*mAipl1*+/−) (*white bar*) and P351Δ12 *hAIPL1*+ (*mAipl1*+/−) (*striped bar*), and the indicated significant differences between both groups to the degeneration model, P351Δ12 *hAIPL1*+ (*mAipl1*−/−) (*gray bar*). *P* values are indicated as follows: $^{*}P < 0.05$. $^{***}P < 0.005$. $^{****}P < 0.0001$.

MATERIALS AND METHODS

Generation of transgenic *hAIPL1* mice

Full-length *hAIPL1* with an N-terminal Flag epitope tag was cloned under the 2.3 kb *mCrx* promoter (15) using a mCrx-LacZ vector generously provided by Dr Takahisa Furukawa (Osaka Bioscience Institute, Osaka, Japan). The P351Δ12 *hAIPL1* mutation was introduced through amplification with reverse primer 5′ CAGCTCTGCAGATGGTGCTGTGGGTGGCTCTGTGGATGACTGTGC 3′, introducing a 12 bp deletion at nucleotide position 1053–1064, and also cloned under the *mCrx* promoter. All polymerase chain reactions (PCR) were performed with Phusion DNA polymerase master mix (Thermo Scientific, Lafayette, CO, USA), following manufacturer instructions for cycling conditions and the sequence verified using Big Dye Terminator ready reaction kit (Perkin Elmer, Waltham, MA, USA). *mCrx-hAIPL1* (WT) and *mCrx*-P351Δ12 *hAIPL1* (mutant) were digested, purified using the Wizard SV Gel and PCR Clean-Up system (Promega, Madison, WI, USA), and injected into the pronuclei of oocytes from superovulated FVB/N females (WVU Transgenic Animal Core Facilities) followed by implantation into pseudopregnant females. WT and mutant P351Δ12 *hAIPL1* transgenic founders were identified through PCR primers amplifying an 750 bp fragment spanning the 3′ region of the *mCrx* promoter and 5′ region of *hAIPL1*, using forward primer 5′ CTGGTTGCAGGCAAGAGT 3′ and reverse primer 5′ GTCCGCTCCTCATCACATTT 3′. Founders were backcrossed into WT 129sv mice to eliminate the *Pde6b*^{rd1} mutation present in the FVB strain, and further backcrossed with *Aipl1* knockout mice in a mixed C57Bl/129sv background described previously (17,21). Mice were maintained under 12-h light/12-h dark light cycles with food and water provided *ad libitum*.

Examination of effects of the mutation in the primate-specific C-terminal region of human AIPL1 necessitated generation of our control WT *hAIPL1* transgenic line. All experiments compared age-matched WT and mutant *hAIPL1* transgenic lines unless explicitly stated. Equal levels of AIPL1 protein expression were present in WT and mutant transgenic animal models prior to retinal degeneration (Fig. 2). Additionally, our control model, WT *hAIPL1* in mouse *Aipl1* knockout background behaved similarly to heterozygous mouse *Aipl1* littermates, previously shown to be without visual dysfunction and retinal degeneration (17). For our double transgenic animal experiments expressing both mutant and WT hAIPL1 alleles, littermate controls were used (Figs 8 and 11).

Immunoblotting and immunocytochemistry

Mice were euthanized by CO_2 inhalation and eyes were enucleated. For immunoblots, flash frozen retinal samples dissected from enucleated eyes were sonicated in phosphate buffered saline (PBS, 137 mM NaCl, 2.7 mM KCl, 4.3 mM Na_2HPO_4·

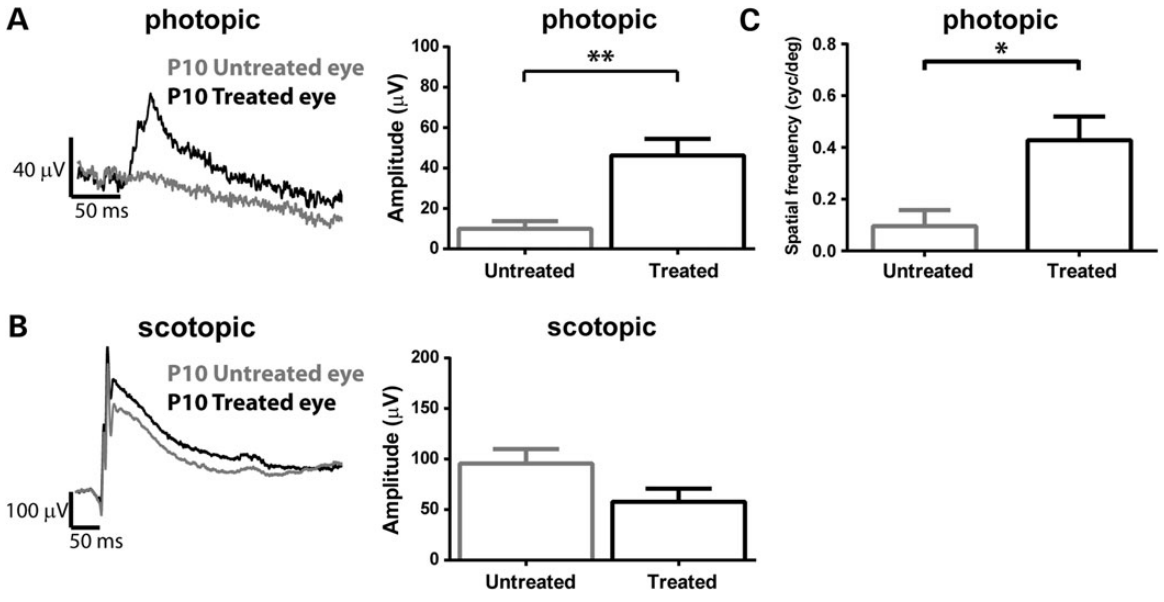

Figure 10. AAV-mediated delivery of WT *hAIPL1* rescued cone-mediated ERG responses and visual function in mutant P351Δ12 *hAIPL1* mice. scAAV2/8-p*RK-hAIPL1* viral vector (21) was administered at P10, introducing non-tagged WT *hAIPL1* into mutant P351Δ12 *hAIPL1* mice ($n = 6$). Treated eyes showed improved (**A**) photopic, cone-mediated ERG responses, but unchanged (**B**) scotopic, rod-mediated ERG responses, when compared directly to its untreated eye. ERG responses were obtained at P30 with 2.5 cd s/m^2 flashes with 30 cd/m^2 rod-desensitizing white background light for photopic, and 2.5×10^{-2} cd s/m^2 flashes for scotopic ERG responses. (**C**) Threshold spatial frequencies (cyc/deg) of the untreated and treated eye from mutant P351Δ12 *hAIPL1* mice that received AAV-mediated gene delivery of WT *hAIPL1* at P10 ($n = 4$), as measured with the OptoMotry system at P30. Bars are mean ± SEM values. *P* values are indicated as follows: $^*P < 0.05$, $^{**}P < 0.005$.

$7H_2O$, 1.4 mM KH_2PO_4, with protease inhibitors and 10 mg/ml dithiothreitol). Protein concentrations were measured using a NanoDrop spectrophotometer (Thermo Fisher Scientific, Inc., Pittsburgh, PA, USA). Furthermore, 150 μg total protein samples were resolved on a 8.7 cm long 10% polyacrylamide sodium dodecyl sulfate-polyacrylamide gel electrophoresis (SDS-PAGE) resolving gel (Criterion Midi format, Bio-Rad, Hercules, CA, USA), or on a longer format 16 cm long 9% polyacrylamide SDS-PAGE resolving gel where specified (Hoefer, Inc., San Francisco, CA, USA), and transferred onto polyvinylidene difluoride membranes (Immunobilon-FL, Millipore, Billerica, MA, USA). Membranes were blocked with blocking buffer (Rockland Inc., Gilbertsville, PA, USA) for 30 min at room temperature and incubated with the indicated primary antibodies. Blots were washed in PBST (PBS with 0.1% Tween-20) twice for 20 min and incubated in secondary antibody, goat anti-rabbit or goat anti-mouse IRDye 680 (LI-COR Biosciences, Lincoln, NE, USA) for 30 min at room temperature. After three washes with PBST, membranes were scanned using the Odyssey Infrared Imaging System (LI-COR Biosciences, Lincoln, NE, USA), and bands quantified using Odyssey Infrared Imaging System software. Quantification of protein levels was conducted on P16 WT ($n = 4$) and mutant *hAIPL1* ($n = 4$) mice with results replicated in three independent studies. In AAV experiments, quantification was between IE and UE in four mice.

For immunohistochemical studies, eyes were immersed in 4% paraformaldehyde fixative for 15 min prior to removal of the anterior segments and lens. The orientation of the eyecup was kept constant by marking at 12 o′clock and sectioned serially dorsal to ventral through the optic nerve head. Eyecups were fixed for an additional 2 h, washed in PBS for 20 min, incubated in 10% sucrose/PBS for 1 h at 4°C and transferred to 20% sucrose/PBS for overnight incubation at 4°C. Eyes were then incubated in 1:1 mixture of 20% sucrose in PBS:optimal cutting temperature (OCT) (Cryo Optimal Cutting Temperature Compound, Sakura, Torrance, CA, USA) for 1 h and flash frozen in OCT. Cryosectioning was performed with a Leica CM1850 Cryostat, and serial retinal sections of 14 μm thickness were mounted on Superfrost Plus slides (Thermo Fisher Scientific, Inc.). Retinal section orientation was kept constant using the 12 o′clock marking and cut sagittally to keep the superior and inferior retina in view. Retinal sections mounted on slides were washed with PBSTx (PBS with 0.1% TritonX-100) and incubated for 1 h in blocking buffer (PBS with 5% goat sera, 0.5% TritonX-100, 0.05% sodium azide). Retinal sections were incubated with primary antibody at the following dilutions overnight at 4°C, followed by three 15 min washes with PBSTx before incubation with secondary antibody (Alexa Fluor-488 or Alexa Fluor-568, Invitrogen, Carlsbad, CA, USA) for 1 h. The nuclear marker 4′,6-diamidino-2-phenylindole (DAPI, Invitrogen, 1:5000 dilution) was added for 10 min and washed with PBSTx before mounting with Prolong anti-fade reagent (Invitrogen). Slides were viewed and imaged on a laser scanning confocal (Zeiss LSM 510) on a Zeiss LSM AxioImager Z1 microscope. Representative immunocytochemistry images are shown from experiments from four animals of each group (WT *hAIPL1*, $n = 4$; mutant *hAIPL1*, $n = 4$) at P16, P35, P70 and P125. In AAV injection experiments, immunocytochemistry images shown are representative of four treated mice.

The following primary antibodies were used at the indicated dilutions: human AIPL1 (1:2500) (17), human and mouse AIPL1 (1:2500) (gift from Dr Tiansen Li, National Eye Institute, Bethesda, MD), Rom1 (1:2000) (gift from Dr Gabriel Travis, UCLA), rhodopsin (1D4, gift from Dr Ted Wensel, Baylor

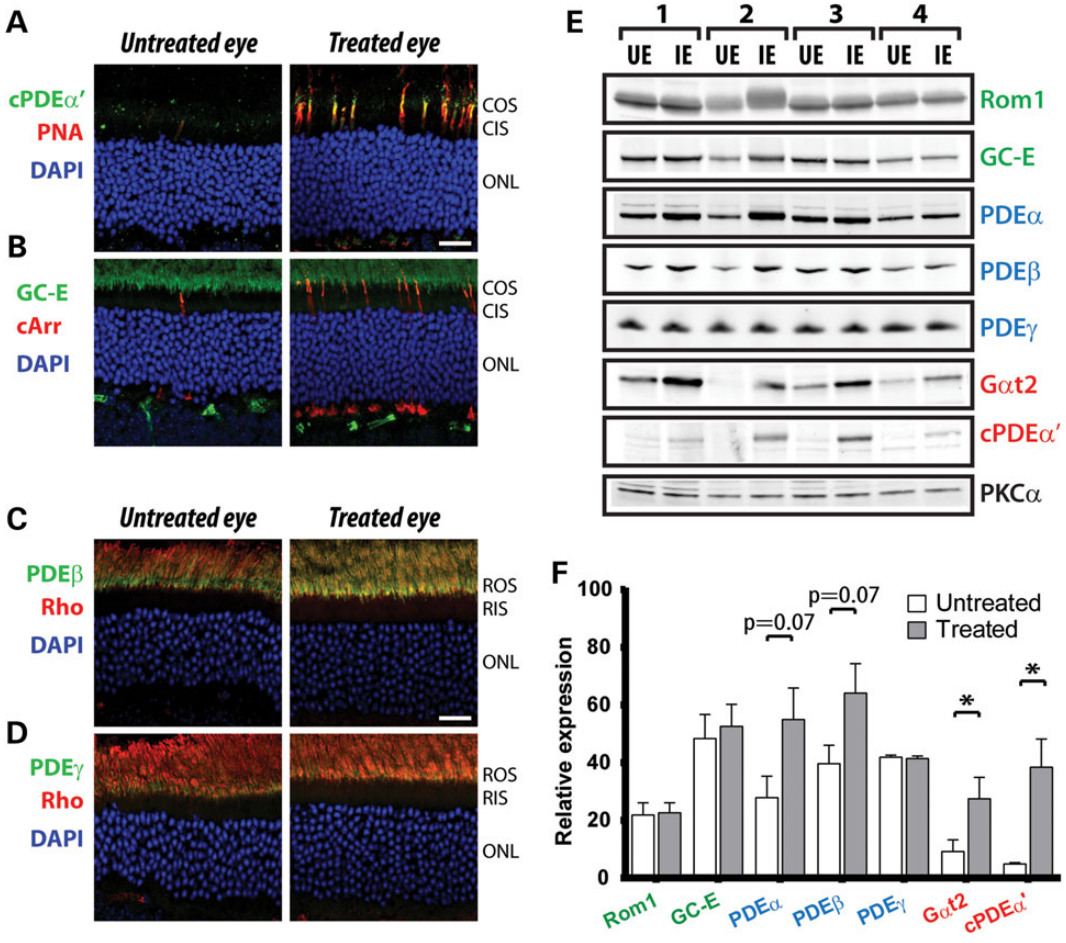

Figure 11. Over-expression of WT hAIPL1 restored cone PDE6 and photoreceptor morphology in mutant P351Δ12 *hAIPL1* mice. Immunocytochemistry of retinal sections from the untreated and treated eye from P130 mice, examining cone rescue with (**A**) cone PDEα′ (*green*) and cone membrane sheath marker, PNA (*red*), (**B**) GC-E (*green*) and cArr (*red*). Restoration of rods and rod-specific proteins were examined with (**C**) PDEβ (*green*) and (**D**) PDEγ (*green*), both co-labeled with rhodopsin (Rho, *red*), present in ROSs. Cell nuclei are stained with DAPI (*blue*). COS, cone outer segment; CIS, cone inner segment; ROS, rod outer segment; RIS, rod inner segment; ONL, outer nuclear layer. Scale bar, 20 μm. (**E**) Immunoblots with (**F**) quantification of protein levels at P130 in the UE and IE from mutant P351Δ12 *hAIPL1* mice that received AAV-mediated gene delivery of WT *hAIPL1* at P10 ($n = 4$). Equal amounts of protein (150 μg) were loaded for each sample, and western blots were probed with the indicated antibodies: Rho, rhodopsin; Rom1, retinal outer membrane protein 1; GC-E, guanylyl cyclase-E; PDEα, cGMP phosphodiesterase 6 α-subunit; PDEβ, cGMP phosphodiesterase 6 β-subunit; PDEγ, cGMP phosphodiesterase 6 γ-subunit; Gαt2, cone transducin α-subunit; cPDEα′, cone cGMP phosphodiesterase α′-subunit; PKCα, protein kinase C α-type.

College of Medicine), red/green opsin (1:1000) (Chemicon, Millipore, Billerica, MA, USA), PDEα (1:2000) (Affinity BioReagents, Golden, CO, USA), PDE6β (1:2000) (Affinity BioReagents), PDEγ (1:2000) (Affinity BioReagents), cone PDE6α′ (1:1000) (16), mouse cArr (IS4) (1:1000) (gift from Dr Wolfgang Baehr, University of Utah, Salt Lake City, UT, USA), GC-E (1:2000) (gift from Dr Baehr) and PKCα (1:2000) (Thermo Fisher Scientific, Inc.). DAPI (1:5000) (Invitrogen, Grand Island, NY, USA), rhodamine PNA (1:2000) (Vector Laboratories, Inc., Burlingame, CA, USA) and PI (1:2000) (EMD Millipore, Billerica, MA, USA) were also used in immunocytochemistry.

Electroretinographic analysis

Mice were dark-adapted overnight prior to testing. Eyes were topically dilated with a 1:1 mixture of tropicamide: phenylephrine hydrochloride. For ERG testing, mice were placed on a heated platform with continuous flow of isoflurane anesthesia through a nose cone (1.5% isoflurane with 2.5 l/min (lpm) oxygen flow rate). A reference electrode was placed subcutaneously in the scalp. ERG responses were recorded from both eyes with silver wire electrodes placed on each cornea, with contact being made with a drop of hypromellose solution (2% hypromellose in PBS) (Gonioscopic Prism Solution, Wilson Ophthalmic, Mustang, OK, USA). Rod-dominated responses were elicited in the dark with flashes of LED white light at increasing flash intensities. Light-adapted cone responses were elicited with white light flashes in the presence of a 30 cd/m^2 rod-saturating white background light. ERGs were performed on the UTAS Visual Diagnostic System with BigShot Ganzfeld with UBA-4200 amplifier and interface, and EMWIN 9.0.0 software (LKC Technologies, Gaithersburg, MD, USA). ERG responses were obtained at P15 (WT *hAIPL1*, $n = 5$; mutant *hAIPL1*, $n = 4$), P30 (WT, $n = 6$; mutant $n = 6$), P60 (WT, $n = 5$; mutant $n = 5$), P90 (WT = 5; mutant, $n = 5$) and P120 (WT, $n = 5$;

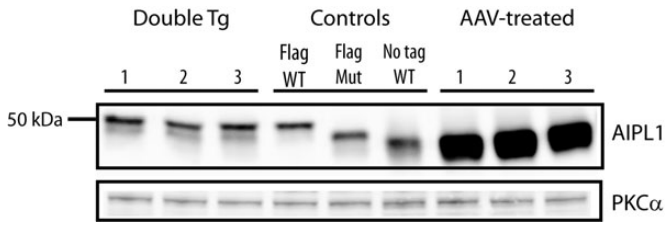

Figure 12. AAV-mediated delivery of *hAIPL1* shows drastically higher expression of WT hAIPL1 than double transgenic animals. Expression of Flag-tagged WT hAIPL1 (*Control: Flag WT* lane), flag-tagged P351Δ12 hAIPL1 (*Control: Flag Mut* lane), and non-tagged WT hAIPL1 (*Control: No tag WT* lane) when probed with anti-AIPL1 (top immunoblot). The protein shows slight band shifts from highest to lowest, respectively, when resolved on a 9% polyacrylamide SDS-PAGE gel of 16 cm height. The control non-tagged WT hAIPL1 sample is from retinal lysate of p*Nrl-hAIPL1* transgenic mice (16). Double transgenic animals were generated by crossing Flag WT *hAIPL1* mice with Flag P351Δ12 *hAIPL1* mice, and retinal lysates from three separate animals are shown (*Double Tg* lanes). Flag P351Δ12 *hAIPL1* mice were administered AAV-mediated gene delivery of non-tagged WT *hAIPL1*, using a scAAV2/8-Y733F-*hAIPL1* viral vector (21), and retinal lysates from three separate animals are shown (*AAV-treated 1, 2, 3* lanes). Retinal lysate from double transgenic mice were age-matched to AAV-treated mice aged P130. Equal protein (150 μg) was loaded for all lanes and loading control is shown with anti-PKCα (bottom immunoblot).

mutant, $n = 5$). In AAV experiments, ERG responses were obtained from treated mice at P30 ($n = 5$), P60 ($n = 5$; *results not shown*) and at P130 ($n = 5$; *results not shown*).

OKRs

Analysis of mouse OKRs were examined using the OptoMotry system (CerebralMechanics, Inc., Lethbridge, Alberta, Canada). Briefly, the system consists of a square array of four computer monitors and an elevated platform on which a freely moving mouse is placed. The mouse is observed from above through a camera mounted at the top. The system was also adapted for measuring OKRs at scotopic light levels, by surrounding the platform with a large cylinder of neutral density filters (E-Color #211 0.9 ND, Rosco Laboratories, Inc., Glendale, CA, USA), and observing the mouse using Night Vision camera mode (Sony, San Diego, CA, USA) under a circular array of six infrared lights (OSRAM Opto Semiconductors, Inc., Sunnyvale, CA, USA), as described previously (20). The computer monitors form a virtual cylinder of rotating sine-wave vertical gratings, which randomly rotates clockwise or counterclockwise as controlled by the OptoMotry computer program. Mice reflexively respond to the rotating gratings by turning their head in the corresponding direction of the grating. The observer registers the mouse behavior through the two-alternative forced-choice protocol by picking either clockwise or counterclockwise (27), and the computer program randomly changes the grating spatial frequency starting from 0.042 cyc/deg (in visual acuity mode, random staircase paradigm) until the threshold or maximal spatial frequency is reached at 70% of the trials (28). Visual acuity was defined as the threshold spatial frequency (cyc/deg). The gratings moved at the optimal speed (S_p) of 12.0 deg/s and temporal frequency (F_t) was automatically adjusted by the computer program based on the equation, $F_t = S_p \times F_s$ (28). Mice were tested with Optomotry at P30 (WT *hAIPL1*, $n = 5$; mutant *hAIPL1*, $n = 5$) and P60 (WT, $n = 5$; mutant, $n = 5$).

Lastly, the OptoMotry apparatus can measure threshold spatial frequency from each eye independently, in a freely moving mouse without any suturing (19). This is because the optokinetic tracking response is elicited when motion is in the temporal-to-nasal direction of the visual field. Thus, counterclockwise grating rotation will drive tracking through the right eye and elicit a counterclockwise OKR; whereas clockwise grating rotation drives tracking through the left eye. This property of the apparatus was taken advantage of to measure treated and untreated eyes in mice receiving AAV-mediated gene delivery. Treated mice were tested with Optomotry at P30 ($n = 4$).

Generation of recombinant AAV vectors

Full-length human *Aipl1* was amplified from pAAV-p*RK-hAIPL1* plasmid (29), and cloned into the scAAV packaging vector (University of Florida, Retinal Gene Therapy Group), to generate the sc-p*RK-hAIPL1* plasmid. The sc-RKp-*hAIPL1* plasmid was used to produce the self-complementary AAV8 Y733F surface-exposed tyrosine residue capsid mutant (scAAV2/8-Y733F-p*RK-hAIPL1*) viral vector described previously (21) with a viral titer of 1.2×10^{13} viral particles per ml.

Subretinal injection for AAV-mediated gene delivery

Transgenic mice injected at postnatal day 10 were placed under general anesthesia with an intraperitoneal injection of ketamine (90 mg kg^{-1})/xylazine (9 mg kg^{-1}) and received a drop of topical anesthetic, proparacaine hydrochloride (0.5%, Akorn, Lake Forest, IL, USA), followed by a drop of dilation solution, consisting of a 1:1 mixture of tropicamide (1%, Alcon, Fort Worth, TX, USA) and phenylephrine hydrochloride (2.5%, Bausch and Lomb, Tampa, FL, USA). Subretinal injection procedures were previously described (21). Sham control injections with 1.25 μl PBS were conducted, and ERG responses either remained the same or reduced from UE. Therefore, all comparisons addressing the efficacy of AAV-treatment were performed with UE as controls. Each animal received 1.25 μl of AAV in the right eye and no injection in the untreated contralateral eye. Visualization during injection was aided by the addition of 0.1% fluorescein (100 mg ml^{-1} AK-FLUOR, Alcon, Fort Worth, TX, USA) to the viral solutions.

Histologic, semi-thin sections and transmission electron microscopy

For light and transmission electron microscopy, mice underwent transcardial fixation perfusion (Tissue Processing and Analysis Core, WVU) prior to retinal sample collection. Briefly, mice were deeply anesthetized with ketamine/xylazine (100 mg/kg ketamine, 10 mg/kg xylazine) prior to perfusion. The animal was perfused through the ascending aorta with a cannula attached to a perfusion pump (Harvard Apparatus, Holliston, MA, USA) with a pressure-relieving incision made in the right atrium. A vascular rinse (Ringer's solution; 154 mM NaCl, 5.6 mM KCl, 2.2 mM $CaCl_2$, 2.4 mM $NaHCO_3$ in 2 mM Tris–Cl, pH 7.4) was conducted prior to perfusion fixation (1% paraformaldehyde, 1.25% glutaraldehyde, 0.1 M sodium cacodylate buffer, pH 7.5). Enucleated eyes were further fixed (2%

paraformaldehyde, 2.5% glutaraldehyde, 0.1 M cacodylate buffer, pH 7.5) for 30 min prior to dissection and removal of the anterior segment and lens, and extensively fixed for 48 h at room temperature. The fixed eyecup was dissected into six to eight wedge-shaped pieces. Wedges were dehydrated in graded ethanol series and then embedded in Polybed 812 (Poly-Sciences, Inc., Warrington, PA, USA). Semi-thin (1 μm) sections were collected onto glass slides, stained with toluidine blue and visualized using a Zeiss Axioimager 2 microscope equipped with EC Plan-Neofluar 40× (NA 0.75) and 100× (1.3 NA) objectives to identify best rescued areas. Thin sections (~80 nm) from selected wedges were collected onto nickel grids, stained with 2% uranyl acetate and lead citrate, and imaged using an FEI Morgagni transmission electron microscope at 80 kV.

Statistics

Statistical analyses were conducted on GraphPad Prism6 software (GraphPad Software, Inc., La Jolla, CA, USA) using two-tailed unpaired *t*-tests for two group comparisons, two-tailed paired *t*-tests for comparisons between untreated and treated eyes in viral rescue studies and one-way ANOVA for multiple group comparisons. Differences were considered statistically significant with $P < 0.05$. Data represent the mean ± SEM and represent the results of at least three independent experiments.

Study approval

All procedures and experiments involving animals described in this study were approved by the Institutional Animal Care and Use Committee at West Virginia University (WVU) and followed the Guide for the Care and Use of Laboratory Animals of the NIH.

SUPPLEMENTARY MATERIAL

Supplementary material is available at *HMG* online.

ACKNOWLEDGEMENTS

We thank Dr Peter Mathers and Ms Ingrid Weterrings of the West Virginia University (WVU) Transgenic Animal Core Facility for their help and services in generating our transgenic lines, Dr Albert Berrebi and the WVU Tissue Processing and Analysis Core for help in mouse transcardial fixation perfusion and Dr Karen Martin of the WVU Microscope Imaging Facility. We are grateful to Drs Vladimir Kefalov and Alexander Kolesnikov at Washington University School of Medicine, St Louis, for generously sharing their expertise in measuring mouse optokinetic responses. We thank Ms Loan Dang at Oakland University for her services and expertise in electron microscopy. Lastly, we thank Drs Wolfgang Baehr at the University of Utah, Tiansen Li at the National Eye Institute, Ted Wensel at Baylor College of Medicine, and Gabriel Travis at University of California Los Angeles for generously providing us with antibodies used in immunohistochemistry and immunoblotting studies.

Conflict of Interest statement. W.W.H. and the University of Florida have a financial interest in the use of AAV therapies, and own equity in a company (AGTC Inc.) that might, in the future, commercialize some aspects of this work.

FUNDING

This work was supported by grants from the National Institutes of Health (EY017035, EY11123, EY08571), West Virginia Lions, Lions Club International Fund, and Unrestricted Challenge Grant from Research to Prevent Blindness (RPB), Macular Vision Research Foundation, and West Virginia Graduate Student Fellowships in Science, Technology, Engineering, and Math (STEM) program.

REFERENCES

1. Daiger, S.P., Bowne, S.J. and Sullivan, L.S. (2007) Perspective on genes and mutations causing retinitis pigmentosa. *Arch. Ophthalmol.*, **125**, 151–158.
2. Foxman, S.G., Heckenlively, J.R., Bateman, J.B. and Wirtschafter, J.D. (1985) Classification of congenital and early onset retinitis pigmentosa. *Arch. Ophthalmol.*, **103**, 1502–1506.
3. Bainbridge, J.W., Smith, A.J., Barker, S.S., Robbie, S., Henderson, R., Balaggan, K., Viswanathan, A., Holder, G.E., Stockman, A., Tyler, N. *et al.* (2008) Effect of gene therapy on visual function in Leber's congenital amaurosis. *N. Engl. J. Med.*, **358**, 2231–2239.
4. Maguire, A.M., Simonelli, F., Pierce, E.A., Pugh, E.N. Jr., Mingozzi, F., Bennicelli, J., Banfi, S., Marshall, K.A., Testa, F., Surace, E.M. *et al.* (2008) Safety and efficacy of gene transfer for Leber's congenital amaurosis. *N. Engl. J. Med.*, **358**, 2240–2248.
5. Hauswirth, W.W., Aleman, T.S., Kaushal, S., Cideciyan, A.V., Schwartz, S.B., Wang, L., Conlon, T.J., Boye, S.L., Flotte, T.R., Byrne, B.J. *et al.* (2008) Treatment of Leber congenital amaurosis due to RPE65 mutations by ocular subretinal injection of adeno-associated virus gene vector: short-term results of a phase I trial. *Hum. Gene Ther.*, **19**, 979–990.
6. Jacobson, S.G., Cideciyan, A.V., Aleman, T.S., Sumaroka, A., Roman, A.J., Swider, M., Schwartz, S.B., Banin, E. and Stone, E.M. (2011) Human retinal disease from AIPL1 gene mutations: foveal cone loss with minimal macular photoreceptors and rod function remaining. *Invest. Ophthalmol. Vis. Sci.*, **52**, 70–79.
7. Testa, F., Surace, E.M., Rossi, S., Marrocco, E., Gargiulo, A., Di Iorio, V., Ziviello, C., Nesti, A., Fecarotta, S., Bacci, M.L. *et al.* (2011) Evaluation of Italian patients with Leber congenital amaurosis due to AIPL1 mutations highlights the potential applicability of gene therapy. *Invest. Ophthalmol. Vis. Sci.*, **52**, 5618–5624.
8. Pennesi, M.E., Stover, N.B., Stone, E.M., Chiang, P.W. and Weleber, R.G. (2011) Residual electroretinograms in young Leber congenital amaurosis patients with mutations of AIPL1. *Invest. Ophthalmol. Vis. Sci.*, **52**, 8166–8173.
9. Tan, M.H., Mackay, D.S., Cowing, J., Tran, H.V., Smith, A.J., Wright, G.A., Dev-Borman, A., Henderson, R.H., Moradi, P., Russell-Eggitt, I. *et al.* (2012) Leber congenital amaurosis associated with AIPL1: challenges in ascribing disease causation, clinical findings, and implications for gene therapy. *PLoS One*, **7**, e32330.
10. Sohocki, M.M., Perrault, I., Leroy, B.P., Payne, A.M., Dharmaraj, S., Bhattacharya, S.S., Kaplan, J., Maumenee, I.H., Koenekoop, R., Meire, F.M. *et al.* (2000) Prevalence of AIPL1 mutations in inherited retinal degenerative disease. *Mol. Genet. Metab.*, **70**, 142–150.
11. Vallespin, E., Cantalapiedra, D., Riveiro-Alvarez, R., Wilke, R., Aguirre-Lamban, J., Avila-Fernandez, A., Lopez-Martinez, M.A., Gimenez, A., Trujillo-Tiebas, M.J., Ramos, C. *et al.* (2007) Mutation screening of 299 Spanish families with retinal dystrophies by Leber congenital amaurosis genotyping microarray. *Invest. Ophthalmol. Vis. Sci.*, **48**, 5653–5661.
12. Walia, S., Fishman, G.A., Jacobson, S.G., Aleman, T.S., Koenekoop, R.K., Traboulsi, E.I., Weleber, R.G., Pennesi, M.E., Heon, E., Drack, A. *et al.* (2010) Visual acuity in patients with Leber's congenital amaurosis and early childhood-onset retinitis pigmentosa. *Ophthalmology*, **117**, 1190–1198.
13. Sohocki, M.M., Bowne, S.J., Sullivan, L.S., Blackshaw, S., Cepko, C.L., Payne, A.M., Bhattacharya, S.S., Khaliq, S., Qasim Mehdi, S., Birch, D.G.

et al. (2000) Mutations in a new photoreceptor-pineal gene on 17p cause Leber congenital amaurosis. *Nat. Genet.*, **24**, 79–83.
14. Dharmaraj, S., Leroy, B.P., Sohocki, M.M., Koenekoop, R.K., Perrault, I., Anwar, K., Khaliq, S., Devi, R.S., Birch, D.G., De Pool, E. *et al.* (2004) The phenotype of Leber congenital amaurosis in patients with AIPL1 mutations. *Arch. Ophthalmol.*, **122**, 1029–1037.
15. Furukawa, A., Koike, C., Lippincott, P., Cepko, C.L. and Furukawa, T. (2002) The mouse Crx 5′-upstream transgene sequence directs cell-specific and developmentally regulated expression in retinal photoreceptor cells. *J. Neurosci.*, **22**, 1640–1647.
16. Kirschman, L.T., Kolandaivelu, S., Frederick, J.M., Dang, L., Goldberg, A.F., Baehr, W. and Ramamurthy, V. (2010) The Leber congenital amaurosis protein, AIPL1, is needed for the viability and functioning of cone photoreceptor cells. *Hum. Mol. Genet.*, **19**, 1076–1087.
17. Ramamurthy, V., Niemi, G.A., Reh, T.A. and Hurley, J.B. (2004) Leber congenital amaurosis linked to AIPL1: a mouse model reveals destabilization of cGMP phosphodiesterase. *Proc. Natl. Acad. Sci. USA*, **101**, 13897–13902.
18. Fulton, A.B. and Rushton, W.A. (1978) The human rod ERG: correlation with psychophysical responses in light and dark adaptation. *Vision Res.*, **18**, 793–800.
19. Douglas, R.M., Alam, N.M., Silver, B.D., McGill, T.J., Tschetter, W.W. and Prusky, G.T. (2005) Independent visual threshold measurements in the two eyes of freely moving rats and mice using a virtual-reality optokinetic system. *Vis. Neurosci.*, **22**, 677–684.
20. Kolesnikov, A.V., Fan, J., Crouch, R.K. and Kefalov, V.J. (2010) Age-related deterioration of rod vision in mice. *J. Neurosci.*, **30**, 11222–11231.
21. Ku, C.A., Chiodo, V.A., Boye, S.L., Goldberg, A.F., Li, T., Hauswirth, W.W. and Ramamurthy, V. (2011) Gene therapy using self-complementary Y733F capsid mutant AAV2/8 restores vision in a model of early onset Leber congenital amaurosis. *Hum. Mol. Genet.*, **20**, 4569–4581.
22. Young, J.E., Vogt, T., Gross, K.W. and Khani, S.C. (2003) A short, highly active photoreceptor-specific enhancer/promoter region upstream of the human rhodopsin kinase gene. *Invest. Ophthalmol. Vis. Sci.*, **44**, 4076–4085.
23. Young, J.E., Gross, K.W. and Khani, S.C. (2005) Conserved structure and spatiotemporal function of the compact rhodopsin kinase (GRK1) enhancer/promoter. *Mol. Vis.*, **11**, 1041–1051.
24. Khani, S.C., Pawlyk, B.S., Bulgakov, O.V., Kasperek, E., Young, J.E., Adamian, M., Sun, X., Smith, A.J., Ali, R.R. and Li, T. (2007) AAV-mediated expression targeting of rod and cone photoreceptors with a human rhodopsin kinase promoter. *Invest. Ophthalmol. Vis. Sci.*, **48**, 3954–3961.
25. Aguila, M., Bevilacqua, D., McCulley, C., Schwarz, N., Athanasiou, D., Kanuga, N., Novoselov, S.S., Lange, C.A., Ali, R.R., Bainbridge, J.W. *et al.* (2014) Hsp90 inhibition protects against inherited retinal degeneration. *Hum. Mol. Genet.*, **23**, 2164–2175.
26. Li, J., Zoldak, G., Kriehuber, T., Soroka, J., Schmid, F.X., Richter, K. and Buchner, J. (2013) Unique Proline-Rich Domain Regulates the Chaperone Function of AIPL1. *Biochemistry*, **52**, 2089–2096.
27. Umino, Y., Frio, B., Abbasi, M. and Barlow, R. (2006) A two-alternative, forced choice method for assessing mouse vision. *Adv. Exp. Med. Biol.*, **572**, 169–172.
28. Umino, Y., Solessio, E. and Barlow, R.B. (2008) Speed, spatial, and temporal tuning of rod and cone vision in mouse. *J. Neurosci.*, **28**, 189–198.
29. Sun, X., Pawlyk, B., Xu, X., Liu, X., Bulgakov, O.V., Adamian, M., Sandberg, M.A., Khani, S.C., Tan, M.H., Smith, A.J. *et al.* (2010) Gene therapy with a promoter targeting both rods and cones rescues retinal degeneration caused by AIPL1 mutations. *Gene Ther.*, **17**, 117–131.